Aus dem Institut Berlin-Brandenburg Center for Regenerative Therapies (BCRT)
der Medizinischen Fakultät Charité – Universitätsmedizin Berlin

DISSERTATION

Ultraschallbasierte Histomorphologie zur nicht-invasiven Klassifizierung der frühen Knorpeldegeneration

Ultrasound based histomorphology for non-invasive grading of early cartilage degeneration

zur Erlangung des akademischen Grades
Doctor rerum medicinalium (Dr. rer. medic.)

vorgelegt der Medizinischen Fakultät
Charité – Universitätsmedizin Berlin

von

Omar Gachouch

Datum der Promotion: 23.03.2024

Contents

List of acronyms and abbreviation

QUS	Quantitative ultrasound
OA	Osteoarthritis
MRI	Magnetic resonance imaging
OCP	Osteochondral plug
TKA	Total knee arthroplasty
SAM	Scanning acoustic microscope
OARSI	Osteoarthritis Research Society International
JSN	Joint space narrowing
KL	Kellgren and Lawrence
FDA	Food and drug Administration
WROMS	Whole Organ Magnetic Resonance Imaging Score
BLOKS	Boston Leeds Osteoarthritis Knee Score
BMLs	Bone marrow lesions
KOSS	Knee Osteoarthritis Scoring System
MOAKS	MR Imaging Osteoarthritis Knee Score
PET	Positron emission tomography
SPECT	Single-positron emission computed tomography
US	Ultrasound
AIB	Apparent integrated backscatter
AFB	Apparent frequency dependence
PBS	Phosphate-buffered saline
NDS	Depth-dependent difference spectrum
ROI	Region of interest
DFS	Depth-dependent frequency spectrum
NBS	Normalized backscattered spectrum
LM	Light microscope
PLS	Partial least squares
SZ	Superficial zone
IRC	Integrated reflection coefficient
TZ	Transitional zone
FS	Full sample

List of figures

List of tables

Abstract

Several studies investigating the assessment of hyaline cartilage degeneration demonstrated that quantitative ultrasound (QUS) is a promising tool to characterize osteoarthritis (OA) changes. Indeed, the cartilage surface reflection and the backscattered ultrasound parameters revealed to be sensitive to early surface and matrix degradation, respectively. However, the majority of these studies were using high-frequency, research-grade single element ultrasound. A method difficult to reproduce clinically. Moreover, only few of them investigated the combination of these parameters. The objective of this study was to propose a quantitative ultrasound-base methodology to predict early osteoarthritis stages using a clinical high-frequency ultrasound system, with a linear array transducer. And to compare its performance to research-grade single-element ultrasound and Magnetic Resonance Imaging (MRI) systems in assessing early OA degeneration.

Osteochondral plugs (OCP) (n=34) of human articular cartilage were collected from patients receiving a total knee arthroplasty (TKA) or cadaver donors. Each OCP was subsequently scanned with a clinical ExactVu Micro-Ultrasound system (Exact Imaging, Markham, ON, Canada), with a nominal center frequency of 29-MHz, a 40-MHz scanning acoustic microscope (SAM), and a Magnetic resonance imaging (MRI) system. QUS parameters related to the surface cartilage, chondrocyte, and collagen changes were computed. The degeneration of each cartilage sample was graded from histology, using the OARSI grading system. The quantitative parameters were correlated to the OARSI cartilage degeneration grade and the histological parameters, individually and in combination.

Results demonstrated that several quantitative parameters from US and MRI were significantly correlated to early OA grade. QUS parameters derived from ExactVu demonstrated a significant correlation with OARSI grade and comparable to MRI parameters ($\rho = 0.75$). The T2 relaxation time from MRI revealed strong significant differences between various groups of OA. A maximum Spearman's rank correlation coefficient (ρ) of 0.82 was achieved using a combination of quantitative MRI and QUS parameters. A maximum ρ of 0.53 and 0.82 were achieved using ExactVu / SAM combination and ExactVu / MRI combination, respectively.

This study demonstrated that a clinical high-frequency ultrasound system, with a linear array transducer, is a promising device to predict early osteoarthritis stages, with results comparable

to research-grade single-element ultrasound and MRI systems. Furthermore, the combination of these systems showed a strong significant correlation with the early OA grade.

Zusammenfassung

Mehrere Studien, die sich mit der Beurteilung der Degeneration des hyalinen Knorpels befassten, haben gezeigt, dass ein quantitativer Ultraschall (QUS) ein vielversprechendes Instrument zur Charakterisierung von Arthrose ist. Die Reflexion der Knorpeloberfläche und die Parameter des rückgestreuten Ultraschalls erwiesen, dass eine frühe Degradation der Matrix vorliegt und eine Veränderung der Oberfläche. In den meisten dieser Studien wurde ein hochfrequenter "Ein-Element-Wandler-Ultraschall" für die Forschung verwendet, dies ist eine Methode, die klinisch schwer zu reproduzieren ist. Außerdem untersuchten nur wenige von ihnen die Kombination dieser Parameter. Ziel dieser Studie war es, eine quantitative ultraschallbasierte Methode zur Vorhersage früher Arthrose-Stadien unter Verwendung eines klinischen Hochfrequenz-Ultraschallsystems mit einem Linear-Array-Schallkopf vorzuschlagen. Und um seine Leistung bei der Beurteilung der frühen Arthrose Stadien mit der Ein-Element-Wandler-Ultraschall- und Magnetresonanztomographie-Systemen (MRT) in der Forschung zu vergleichen.

Die Osteochondralen Stanzbiopsien (n=34) wurden aus menschlichem Gelenkknorpel entnommen, von Patienten, die eine Knie-Totalendoprothese erhielten oder von Leichenspendern. Jedes OCP wurde anschließend mit einem klinischen ExactVu-Mikro-Ultraschallsystem (Exact Imaging, Markham, ON, Kanada) mit einer nominalen Mittenfrequenz von 29 MHz, einem akustischen Rastermikroskop mit 40 MHz und einem Magnetresonanztomographiesystem untersucht. QUS-Parameter, die sich auf die Veränderungen des Oberflächenknorpels, der Chondrozyten und des Kollagens beziehen, wurden somit berechnet. Die Degeneration jeder Knorpelprobe wurde anhand der Histologie nach dem OARSI-Grading-System bewertet. Die quantitativen Parameter wurden mit dem OARSI-Knorpeldegenerationsgrad und den histologischen Parametern korreliert, sowohl einzeln als auch in Kombination.

Die Ergebnisse zeigten, dass mehrere quantitative Parameter aus US und MRT signifikant zusammenhängen mit dem frühen Arthrose Stadium. Die aus ExactVu abgeleiteten QUS-Parameter zeigten eine signifikante Korrelation mit dem OARSI-Grad und waren mit den MRT-Parametern vergleichbar (ρ = 0,75). Die T2-Relaxationszeit der MRT zeigte starke signifikante Unterschiede zwischen den verschiedenen Arthrose Stadien. Mit einer

Kombination aus quantitativen MRT- und QUS-Parametern wurde ein maximaler Spearman's Rank-Korrelationskoeffizient (ρ) von 0,82 erreicht. Ein maximaler ρ-Wert von 0,53 bzw. 0,82 wurde mit der ExactVu/SAM-Kombination bzw. der ExactVu/MRT-Kombination erreicht.

Diese Studie hat gezeigt, dass ein klinisches Hochfrequenz-Ultraschallsystem mit einem Linear-Array-Schallkopf ein vielversprechendes Instrument zur Vorhersage früher Arthrose-Stadien ist, mit Ergebnissen vergleichbar mit einem MRT-System. Darüber hinaus zeigte die Kombination dieser Systeme eine starke signifikante Korrelation mit dem frühen Arthrose Stadium.

1 Introduction

Articular cartilage is a specialized, non-vascularized, and non-innervated tissue located on the surface of the bone. It allows, through its mechanical properties of resistance and elasticity, the sliding of bone surfaces with a low coefficient of friction. Healthy cartilage is composed of a single type of cell, chondrocytes, located within a dense extracellular matrix, and has a characteristic depth-dependent architecture. Chondrocytes are spherical or ovoid in shape, measuring 30 to 40 μm in diameter, and occupying 2% of the total volume of the cartilage. The extracellular matrix (65-80% water, 20-35% macromolecules) is organized into a network rich in type II collagen fibers, where macroaggregates of proteoglycans are trapped. There are generally four layers in the cartilage (Figure 1). A surface layer (10% to 20% of the cartilage volume), where small and flat chondrocytes and collagen fibers are arranged parallel to the surface. The special arrangement of this zone allows resistance to tensile forces and protects the deeper layers. This area is relatively poor in proteoglycans. An intermediate layer where the chondrocytes are large, spherical, and distributed randomly between the collagen fiber without particular orientation. This zone represents 40% to 60% of the full thickness of the cartilage and provides a connection between the superficial and radial zones. A deep or radial layer, where the chondrocytes are even larger and arranged in columns along with thick collagen and arranged perpendicular to the surface. The concentration of proteoglycans is the highest and that of water is the lowest in this area. This organization provides resistance to compressive forces. The fourth layer, finally, in contact with the subchondral bone plate, which is mineralized, is called the calcified zone and distinguished from the deep zone by the tide mark (1).

Osteoarthrosis (OA) is one of the most prevalent and disabling joint diseases, which degenerates hyaline cartilage (2), and affected 303 million people in the world in 2017 (3). Over 50 million of the population in Europe are believed to be affected by the disease, or around 7% of the population (4). The incidence in 2017 was estimated at nearly 15 million worldwide, and more than 2 million in Europe. According to the Robert Koch Institute, the disease affects 17.9% of the adult population in Germany, with a prevalence of 21.8% for women and 13.9% for men (5). Its prevalence is strongly correlated with age: more than 48% of OA women patients and 31% of OA men patients are over 65 years old. As stated by the United Nations, three times more people will be affected by the disease at the age of 60 (6). This represents more than 20% of the world's population, and 40 million people will be severely disabled. The

OA manifests itself first with joint pain, and up to a major disability with loss of mobility. It has a considerable impact on life quality and causes the greatest burden for the population in terms of pain and disability, up to surgical management (joint prosthesis) for the most severe cases. The 2017 Global Burden of Disease Study published that the concern of osteoarthritis has considerably increased these past 10 years, and has become one of the leading causes of years lived with disability (7). The economic burden on patients and society is also consequential. A systematic review of the literature estimated the average direct and indirect cost per patient to 8500 euros/year (8). Besides other consequences, such as reduced productivity, premature dismissal, or autonomy loss. The high utilization of hospital facilities and surgery for osteoarthritic patients results in a considerable financial burden. In 2008, the evaluation of the direct costs of the treatment of the pathology was estimated at 7.62 billion euros in Germany (9), and these applications caused more than $60 billion each year in the US (10). OA is a pathological process strongly related to age, but also metabolic disorders, such as diabetes or cardiovascular disease (11). Even if the mechanism is not totally understood, several meta-analyses highlighted an association between Osteoarthrosis and metabolic syndromes.

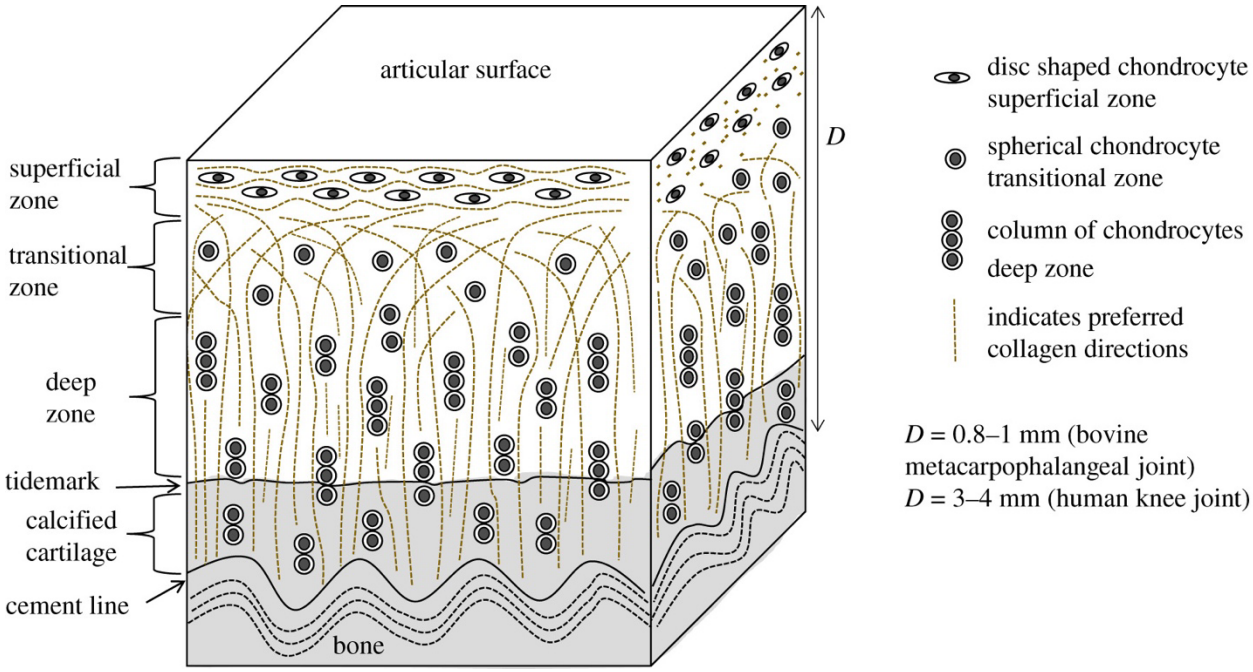

Figure 1: Structure of healthy human articular cartilage (12). Superficial zone: small and flat chondrocytes, cells and collagen fibers arranged parallel to the surface. Middle zone: round chondrocytes and collagen fibers distributed randomly. Deep zone: round chondrocytes arranged in columns and collagen fibers perpendicular to the surface. With permission from Royal Society Publishing. Available from: https://royalsocietypublishing.org/doi/10.1098/rsif.2018.0611

Osteoarthritis is a heterogeneous disorder, and as mentioned by Kraus et al. in their review, the importance of a standardized definition and description of the disease to stimulate the development of efficient diagnosis tools (13). According to their definition, "Osteoarthritis is a disorder involving movable joints characterized by cell stress and extracellular matrix degradation initiated by micro and macro-injuries that activate maladaptive repair responses including pro-inflammatory pathways of innate immunity. The disease manifests first as a molecular derangement (abnormal joint tissue metabolism) followed by anatomic, and/or physiologic derangements (characterized by cartilage degradation, bone remodeling, osteophyte formation, joint inflammation, and loss of normal joint function), that can culminate in illness" (13). We can read in this definition that OA can manifest itself on different levels, molecular, anatomic, and physiologic. However, these manifestations do not occur at the same period. Molecular changes can reveal abnormalities several years before the first anatomical or physiological indicators, causing a long asymptomatic state of the disease. The progression of OA is characterized by morphological and biomechanical changes in chondrocytes and matrix, which destabilize the balance between the synthesis and the degradation of cartilage (13). These changes lead to softening, fibrillation, cracking and loss of joint cartilage. First, an increase, followed by a decrease in the proteoglycan concentration, combined with an increase in the water concentration, results in tissue softening. This will cause fibrillation of the superficial zone of the cartilage, and then deeper and deeper fissures until reaching the subchondral bone. In parallel, a proliferation of chondrocytes that increase their activity is observed, the objective of this hypercellularity is to repair the damage by synthesizing matrices. But the anabolic activity and the proliferation of chondrocytes will decrease, leading to a hypocellularity, an apoptotic process, a disruption of the collagen network, and a progressive destruction of the cartilage. Histological analysis, the current gold standard, using different scoring methods, such as the OARSI grading system (14) (Table 1), can verify these changes (Figure 2).

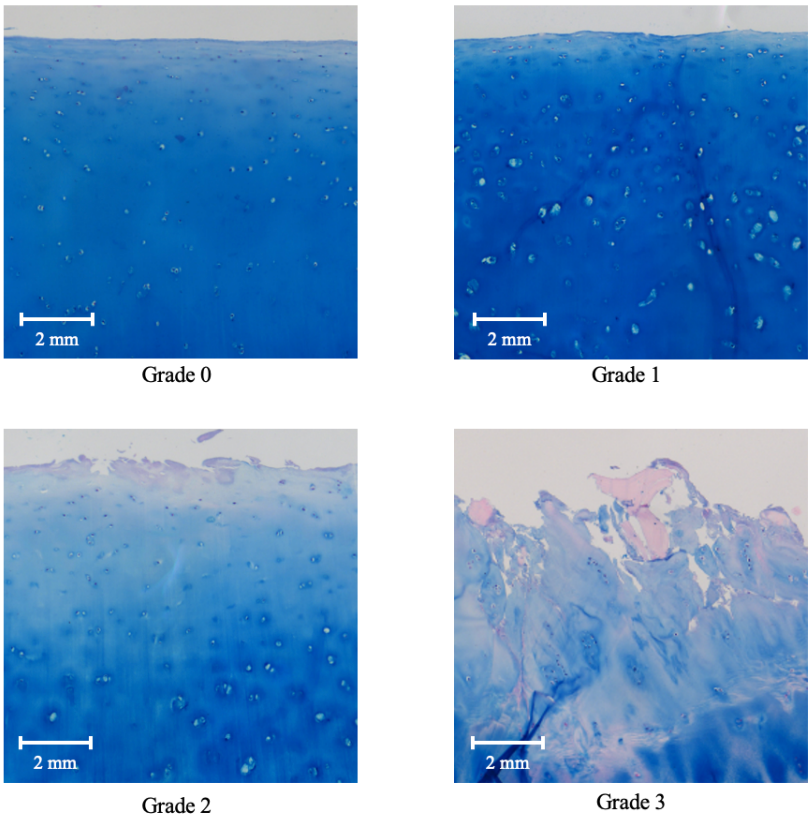

Figure 2: Histological changes of early osteoarthritis cartilage degeneration. Five micrometer paraffin sections of cartilage stained by Alcian blue and Nuclear fast red-aluminum sulfate. Pictures taken with 40x light microscope objectives. Grade 0: surface intact, matrix normal and cells intact. Grade 1: superficial fibrillation, cells proliferation (clusters). Grade 2: surface discontinuity, Matrix discontinuity at superficial zone, cells death and clusters, Alcian blue staining depletion (transitional zone). Grade 3: matrix vertical fissures into transitional zone, cells death, Alcian blue staining depletion (deep zone) (14). Own Creation.

The diagnosis of osteoarthritis is mostly based on conventional radiographic imaging, and clinical approaches, by evaluating symptoms, such as pain, in combination with assessing the patient's health history (15). The anatomical lesions are easily revealed by x-ray, as soon as the lesions are advanced. In that case, a narrowing of the space between the bones, a pinching of the joint space, the presence of osteophytes or subchondral bone condensation can be identified. The joint space narrowing (JSN) is the main mark, used by the semi-quantitative Osteoarthritis Research Society International (OARSI) classification to evaluate the OA progression (15, 16). Other anatomical lesions are used in different semi-quantitative scoring methods to assess the severity of OA. Such as the Kellgren and Lawrence (KL) grading system, based on the presence of osteophyte (16). But also, quantitative scoring methods, using for example joint space width (JSW). Each of these methods has its own limitations, and cannot grade properly OA, even less detecting the early or mild signs. Despite their limitations, conventional radiography remains the gold standard to establish a diagnosis of OA. And the

only imaging-based modality approved by the U.S. Food and Drug Administration (FDA), for the assessment of structural modification and to demonstrate the efficacy of new drugs and regenerative therapies in clinical trials (15). However, at the time symptoms become apparent, OA is usually already advanced and cannot be reversed or healed, which limits efficient treatment and therapy. Nowadays, none of the established imaging methods is precise enough to assess these degenerative tissue damage, and predict the progression of osteoarthritis. It is evaluated clinically and radiologically with the study of the progression of these different lesions. That makes the detection of early signs, and a more effective treatment of the disease impossible. Hence, a non-invasive device that is capable of detecting early signs of osteoarthritis before symptoms appear would allow better management of the disease.

Additionally to radiography, arthroscopy is a conventional method widely used for the diagnosis of joint damage. It is a minimally invasive surgical technique. The intervention is characterized by the insertion at the joint level of a fiberoptic endoscope connected to a camera. This method enables quick visualization of the cartilage and allows surgical proceedings. This operation can have a diagnostic or therapeutic purpose. Although the surgery involves only minimal incisions, it is performed in an operating room and under anesthesia. Arthroscopy can diagnose lesions of the meniscus or articular cartilage, but its use is more frequently interventional: repair or removal of the meniscus, smoothing the surface of the cartilage, reconstruction of the ligaments, biopsies, joint washing, and removal of fragments cartilaginous. Furthermore, recent studies have shown the possibility of assessing cartilage by using intravascular or intra-articular ultrasound during arthroscopy (17). However, several meta-analyses and systematic reviews questioned the benefits of using arthroscopy for degenerative knee disease, and consider it even as a high risk of subsequent knee replacement (18).

Magnetic resonance imaging (MRI) is getting more attractive, as it can assess changes in soft tissue and bone, unlike conventional radiography. It is showing great imaging capabilities for diagnosing OA and will have a role in the future in OA monitoring and treatment planning. Several semi-quantitative MRI methods for the scoring of OA are already validated and standardized, such as WORMS, BLOKS, MOAKS, KOSS, and more recently OMERACT and KIMRISS (15, 16). These scoring systems assess diverse structural damage associated with OA in cartilage morphology and composition, bone marrow lesions (BMLs), osteophytes, and the menisci (19). More specifically, the Whole Organ Magnetic Resonance Imaging Score (WROMS) and the Boston Leeds Osteoarthritis Knee Score (BLOKS) are the most investigated

and used systems. Both are based on the scoring of BMLs, osteophytes, subchondral cysts, synovitis, meniscus, ligament. The Knee Osteoarthritis Scoring System (KOSS) is also widely known and used. But all have weaknesses that the MR Imaging Osteoarthritis Knee Score (MOAKS) tries to correct, by refining the scoring of BLMs and meniscus. Besides, several studies have shown that quantitative MRI parameters are related to different contents involved in the organization of the cartilage, and a strong sensitivity to cartilage degeneration changes. Furthermore, compositional MRI may be sensitive to early and mild signs of OA progression. As suggested, T2 quantifies collagen network integrity and water contents (20, 21). T1ρ and T2ρ are related to bone lesions, proteoglycan loss, collagen disorganization (22), and dGEMRIC linked to the concentration of glycosaminoglycans (23). These values were able to differentiate early and advanced stages of osteoarthritis and were correlated to histological results. Nevertheless, these methodologies using quantitative MRI are not yet accessible for clinical use, and the MRI is also not used in a clinical routine to diagnose OA, as it is an expensive modality and artifacts can mimic pathological changes.

CT has shown great results in assessing bone or joint abnormalities, such as facet joints of the spine, or evaluating cysts, erosions, and osteophytes associated with OA. But the constraints of imaging soft tissue and the high radiation dose, thus limited this modality to extract information for assessing fully osteoarthritis (16). CT arthrography, however, using intra-articular contrast techniques, enables the evaluation of articular cartilage damage with a high anatomic resolution. The high spatial resolution and the high contrast make this technique the most accurate method to determine cartilage thickness. As well as detecting superficial lesions with high accuracy, to characterize bone sclerosis and osteophytes. But this method is barely used due to the importance of its limitations (expensive and invasive). Scintigraphy, Positron emission tomography (PET), and Single-positron emission computed tomography (SPECT) are three nuclear medical modalities described in the literature on their potential of assessing OA (15). The first one helps to detect the area of pain for patients with complex symptoms. The second one, PET, showed synovitis and bone marrow lesions (BMLs) association with OA. And the last one, SPECT, in combination with radiopharmaceutical agents showed an association of cartilage damage and the decrease of this agent. But all these techniques are still limited compared to conventional radiography, MRI, or Ultrasound, in assessing OA, due to their invasive nature, high cost, or technical limitations. The combination of CT or MRI and PET would reduce some of the limitations, such as poor resolution and ionizing radiation, but few clinical studies have been done.

Table 1: OA cartilage histopathology grade assessment – advanced grading methodology. Reused from (14) with permission from Elsevier.

Grade (key feature)	Subgrade (optional)	Associated criteria (tissue reaction)
Grade 0: surface intact, cartilage intact	No subgrade	Intact, uninvolved cartilage
Grade 1: surface intact	1.0 Cells intact 1.5 Cell death	Matrix: superficial zone intact, edema and/or fibrillation Cells: proliferation (clusters), hypertrophy Reaction must be more than superficial fibrillation only
Grade 2: surface discontinuity	2.0 Fibrillation through superficial zone 2.5 Surface abrasion with matrix loss within superficial zone	As above +Discontinuity at superficial zone ±Cationic stain matrix depletion (Safranin O or Toluidine Blue) upper 1/3 of cartilage (mid zone) ±Disorientation of chondron columns
Grade 3: vertical fissures	3.0 Simple fissures 3.5 Branched/complex fissures	As above ±Cationic stain depletion (Safranin O or Toluidine Blue) into lower 2/3 of cartilage (deep zone) ±New collagen formation (polarized light microscopy, Picro Sirius Red stain)
Grade 4: erosion	4.0 Superficial zone delamination 4.5 Mid zone excavation	Cartilage matrix loss, cyst formation within cartilage matrix
Grade 5: denudation	5.0 Bone surface intact 5.5 Reparative tissue surface present	Surface is sclerotic bone or reparative tissue including fibrocartilage
Grade 6: deformation	6.0 Joint margin osteophytes 6.5 Joint margin and central osteophytes	Bone remodelling. Deformation of articular surface contour (more than osteophyte formation only) Includes: microfracture and repair

Ultrasound techniques for medical diagnosis are distinguished from many medical imaging techniques by their non-injurious nature. These techniques can be used iteratively and without risk for the patient, and provide morphological and functional information. Ultrasound techniques have a very high spatial and temporal resolution, with performance superior to all other modalities. Ultrasound is a mechanical wave, local pressure variations propagating in materials (fluids and solids) without transporting materials. The wave propagation depends on the elastic properties and mass density of the material. It is a sound with a frequency between 20 kHz and 200 MHz, which is not perceptible to the human ear. The ultrasonic wave is characterized by its frequency (f), period (T), amplitude, and wavelength (λ). The wavelength depends on the speed (c) of ultrasound propagation, which varies depending on the environment and distinguishes the tissues.

$$\lambda = \frac{c}{f} = cT \tag{1}$$

On average, in living biological tissues, the speed of ultrasound propagation is equal to 1540 m/s. When transmitted through tissue, the ultrasonic wave encounters media with different physical characteristics. These differences can be expressed in terms of mass density (ρ), ultrasound propagation speed, and acoustic impedance (Z).

$$Z = \rho . c \tag{2}$$

When the ultrasound wave passes through biological tissue, it can result in different types of interactions, such as attenuation, absorption, reflection, and scattering (Figure 3). Reflection occurs on all surfaces between two media or tissues (interface) with different acoustic impedances or speeds of sounds (24). The greater this difference is, the higher the proportion of acoustic energy is reflected, the proportion of transmitted acoustic energy decreases then. When forming ultrasound imaging, specular reflection is responsible for displaying tissue boundaries. The propagation of the ultrasonic wave is not always straightforward. It can in fact be deviated from its trajectory by refraction, deflection of the ultrasonic beam that occurs when an interface is reached by the beam at oblique incidence. The attenuation of ultrasound can be explained by two main mechanisms; absorption and scattering and is broadly proportional to the distance traveled. In a homogeneous environment, the acoustic intensity decreases exponentially with distance, along with the ultrasound frequency. The result of this attenuation is a transformation of acoustic energy into heat. Depending on the properties of the material, absorption can be explained by several phenomena (chemical or thermal mechanisms, viscosity of the medium…). Scattering is caused by the interaction of the ultrasonic wave and particles surfaces. The effect resulting from this interaction is the dispersion of the incident energy in all directions of space, and constitutes the basis of ultrasonic imaging formation. It occurs when the size of the scatterer is equal or smaller than the ultrasonic wavelength. The scattering in the direction of the incidence wave source is called backscattering.

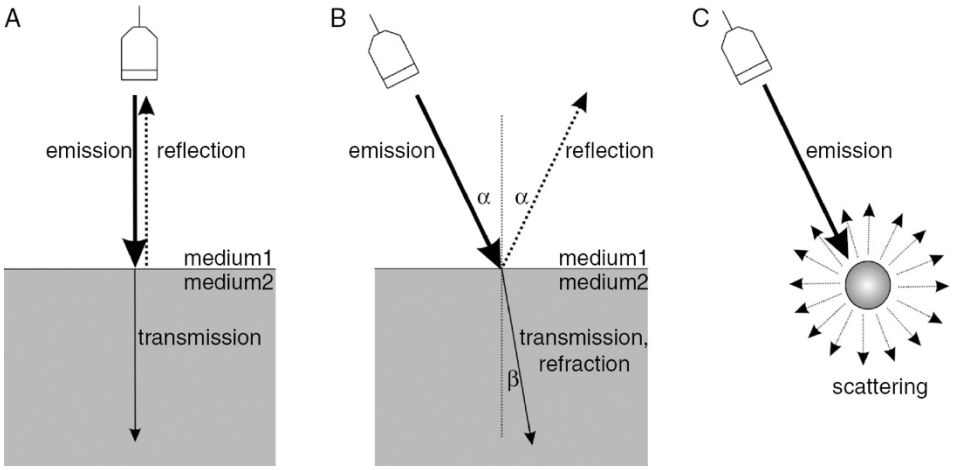

Figure 3: Interactions of a plane wave at the boundary of two medium. (A) reflection and transmission, (B) Refraction and (C) scattering (Oláh et al. 2016). Reuse from (25) with permission from Cambridge University Press

Clinical Ultrasound has some advantages in the assessment of musculoskeletal diseases compared to the imaging systems developed above. Being a low-cost, non-invasive, portable, and non-ionizing imaging modality makes it attractive for in vivo diagnosis and monitoring

treatment response. A recent systematic review sums up the potential of US in the imaging of relevant features to OA, such as the visualization of synovitis without contrast agents, the detection of osteophytes, meniscus extrusion, or femoral trochlear cartilage (26). Publications of the past decades indicate that quantitative ultrasound parameters have a great potential in providing a tool for assessing hyaline cartilage degradation and predicting stages of osteoarthritis. It was demonstrated that several spectral parameters from cartilage surface and backscattered ultrasound are sensitive to morphological properties of articular cartilage that are related to early signs of OA. The most established ones from cartilage surface are surface reflection amplitude and surface roughness, associated with matrix stiffness and roughness (27). Likewise, it was shown that different cartilage degeneration stages are correlated to backscattered ultrasound parameters extracted from the cartilage extracellular (28, 29). The most studied quantitative parameters are the apparent integrated backscatter (AIB), which is the integrated backscattered energy over the transducer bandwidth, sensitive to matrix composition, cellular structure, and cartilage degeneration (30, 31). And the apparent frequency dependence of the backscatter amplitude (AFB), which assumed to predict for the early degenerative stages of OA (32).

Another study suggested that parameters from quantitative ultrasound signals can be related to chondrocyte changes (31). The regular spacing of cell layers in the superficial zone of healthy articular cartilage showed to be represented by a resonance peak, caused by the coherent backscatter content of the ultrasound signals, due to the regular arrangement. We can expect that the morphological changes in the organization of the cell in the superficial layer, due to early signs of degeneration can have an impact on the backscattered frequency spectrum. This disorganization can lead to the loss of this coherent component of the scattering. The combination of these parameters and their derivatives are related to matrix composition, cell number density, and degree of cartilage degeneration.

The majority of the studies mentioned above have used high-frequency single-element ultrasound transducers, developed for research. Thus, the goal of this project is to propose a new methodology, based on quantitative ultrasound, and clinically suitable, for assessing hyaline cartilage degradation and predicting early stages of osteoarthritis (OA). That is why, QUS parameters related to the surface cartilage, chondrocytes, and collagens changes were investigated using a high-frequency linear array ultrasound transducer. We hypothesize that apoptotic chondrocytes will differ from healthy cells in the acoustic properties and therefore will have an impact on the backscattered ultrasound signals. Indeed, we consider that the

parameters related to chondrocyte morphology and organization can be precisely evaluated by extracting ultrasound backscatter, correlated with the progression of OA, and distinguishing the early and late stages. The well-established and novel QUS parameters were also extracted from a 40 MHz custom-made scanning acoustic microscope, using a single-element, spherically-focused transducers, for comparison. In addition, quantitative parameters were extracted from data provided by a MRI system to compare the performance of this new methodology.

2 Material and Methods

2.1. Samples

For this study, 36 punch biopsies were collected from the medial tibial plateau or the lateral femoral condyle. Among which, 34 samples are from patients receiving a total knee replacement surgery (TKA) with mild visible signs of matrix destruction. The samples were selected by an expert clinician during the surgery. As well as 2 samples were selected from donors with no visible signs of matrix destruction (post-mortem). The first one died from an alcoholic liver injury and the second one from a myocardial infarction. In the load-bearing regions of the biopsies, 6.mm osteochondral plugs (OCP) were extracted using a hollow drill (Bosch PBD 40), and then stored in a solution composed of phosphate-buffered saline (PBS) and an inhibitor of proteolytic enzymes, 5mM benzamide HCl (Sigma-Aldrich, St. Louis, MO, USA), to prevent degradation. Approval for the experiments was granted from the ethics commissions of the Charité-Universitätsmedizin Berlin (Protocol EA2/208/18) and approved by the local institutional review boards.

2.2. Ultrasound scanning and post-processing

After extraction of the OCP from the punch biopsy, all samples were scanned the same day. First, using a clinical ExactVu Micro-ultrasound system with a 29-MHz linear array transducer (Figure 4B). This medical device is a clinical system built for clinical urological applications, FDA approved for imaging prostate cancer, and enables high-resolution imaging. In this study, the ExactVu system was used to investigate the feasibility of detecting cartilage degeneration using a clinical system. The samples were placed in a Teflon holder filled with PBS and covered with a thin membrane made of Parafilm M (Merck, Darmstadt, Germany). The holder was fixed to a water tank with a manual stage, to position the surface of the cartilage samples parallel to the side-fire transducer. The tank was filled with degassed water at 37 °C. Prior scanning, the holder was kept 30 min in the degassed water to adjust the temperature of

the cartilage sample to the bath (Figure 4A). Successive B-mode images (gain: 55-dB, dynamic range: 65-dB) (Figure 4C) were performed in 2 different focusing (10-mm and 15-mm), to allow 3D reconstruction and measurements, with the following settings: scan increment of 0.25-mm, number of increments of 40 planes. To realize these measurements, the transducer of the ExactVu system was fixed to a motorized linear translation stage (MTS50-Z8, Thorlabs, Newton, NJ, USA) and connected to a motor controller (KDC101, Thorlabs, Newton, NJ, USA) to allow the navigation and aligned the transducer to the sample. All these components were controlled by a custom software developed on MATLAB (MATLAB R2018a, MathWorks, Natick, MA) using an Advanced Positioning Technology method (APT 3.21.4, Thorlabs, Newton, NJ, USA), and installed on the ExactVu system desktop.

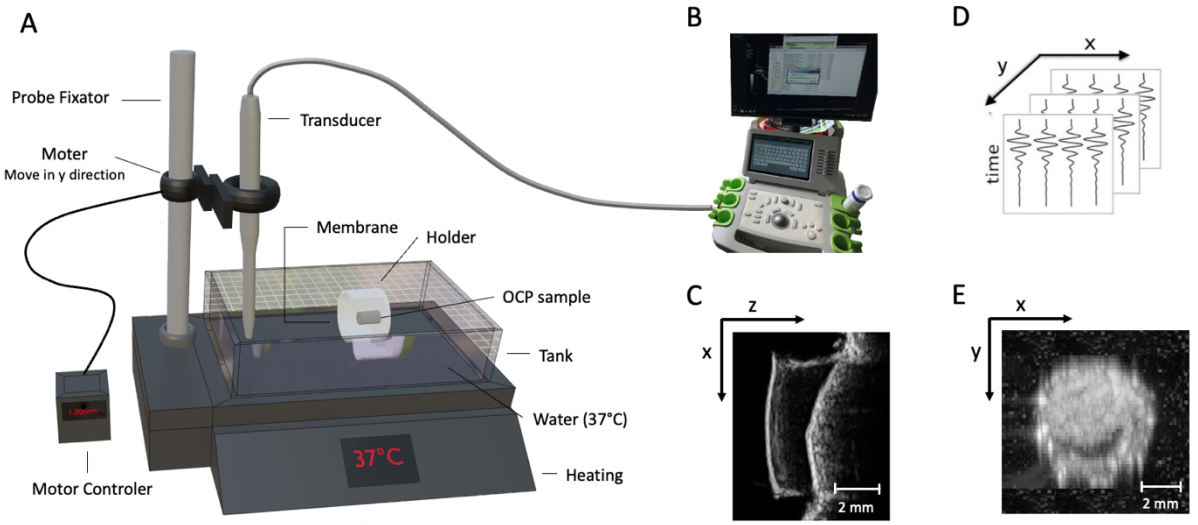

Figure 4: (A) Illustration of the setup for the ExactVu experiment. (B) ExactVu Micro-ultrasound system with a 29-MHz transducer. (C) Representative B-mode image of an osteochondral samples (OCPs). (D) Set of time resolved signal obtained with a successive B-mode images. (E) Representative surface reflection map of an osteochondral sample (OCP). Own Creation.

Then, the samples were scanned using a custom scanning acoustic microscope SAM200Ex. Introduced by Lemons and Quate in 1974, the scanning acoustic microscope has repeatedly shown its interest to image biological structures with high spatial and lateral resolution (33). In this setup, SAM was used with a spherically focused 40-MHz single element transducer (Figure 5A), The transducer's specifications have been reported in detail in a previous study (28). The system is built on a high-precision motion stage to allow the navigation of the transducer in the three spatial dimensions (x, y, z). During the motion, for each fixed position, an excitation signal is generated by a pulser activated by an AD-card. Then a reflected signal is processed by a receiver and digitized by the AD-card. All these components are controlled by a custom C++ software (SAM200Ex, Q-BAM, Halle, Germany). The samples

were positioned in a tank, parallel and aligned to the transducer, and immersed with degassed PBS at a constant temperature of 37 °C. The samples were kept for 20 min in the PBS bath to adjust the temperature of the cartilage sample to the bath. When the confocal position of the transducer was reached, the samples were measured in time-resolved C-scan mode, using a scan increment of 40 µm in the x and y directions (Figure 5B).

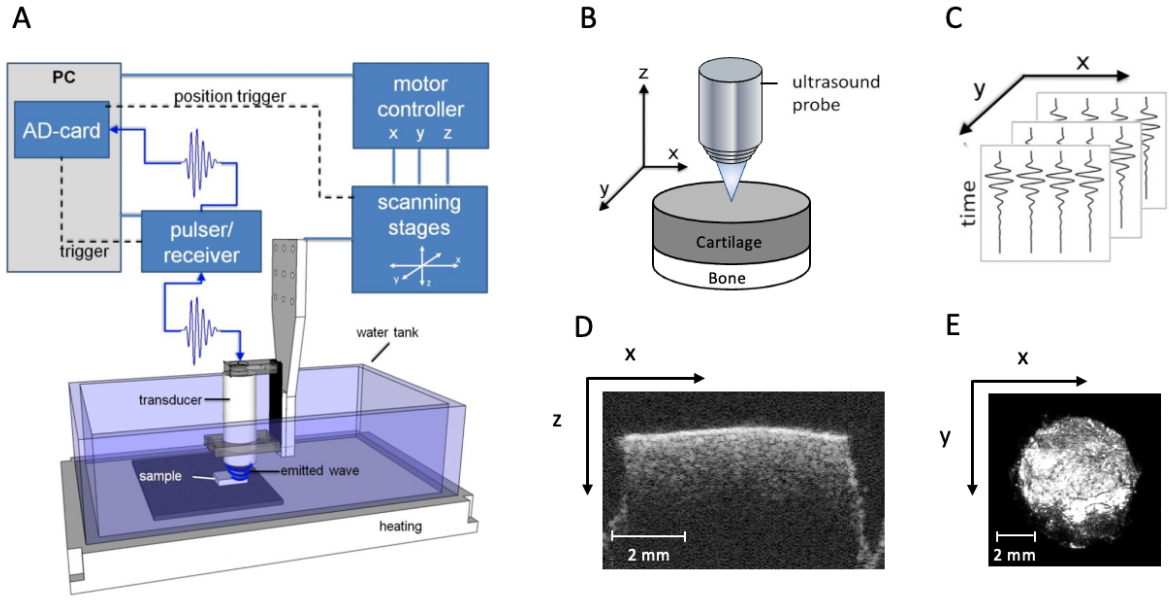

Figure 5: (A) Illustration of the Scanning acoustic microscope (SAM) setup. (B) Schema using a C-scan mode with SAM. (C) Set of time resolved signal obtained with a C-scan. (D) Representative B-mode image of an osteochondral sample (OCP). (E) Representative surface reflection map of an osteochondral sample (OCP). Adapted from (34) with permission from Dr. Rohrbach.

These two ultrasound systems were used to evaluate the backscatter spectrum from the superficial zone of the cartilage samples. The normalized depth-dependent difference spectrum (NDS) was computed in a similar way as previous studies (31, 35). Subsequently the surface was detected using thresholding and spatial filtering methods. The region of interest (ROI) (1.0 mm x 1.0 mm) was selected manually in the lateral direction, in the center of the cartilage sample. The region of interest in this study was moderately bigger than the ROI of the previous studies (29, 31), offering a better representation and image quality of the cartilage structure. Then, the depth-dependent frequency spectrum (DFS), a 2D function of frequency and depth from the surface, was computed. The DFS was obtained by calculating the power spectra of each filtered RF signal in an axial overlapped time gate and laterally averaged in both directions over the ROI. In previous studies, each time gate had a length of 117 ns with an axial overlap of ~90%, while the time gate in this study had a length of 125 ns and an axial overlap of ~90%. The slight difference in time gate length can be explained by the transducer used for the measurements, leading to a different bandwidth. The bandpass filter used to reduce the noise

was a type II Chebyshev filter with cutoff frequencies of 5 and 80 MHz, and 3 and 28 MHz, for SAM200Ex and ExactVu, respectively. Finally, the NDS was obtained by dividing a reference spectrum at each depth of the DFS. In previous studies, a planar reflector (polymethylmethacrylate) was used as a reference spectrum to compensate for the effects of system and transducer transfer functions, and/or an agar graphite phantom to correct the defocus amplitude decrease and diffraction effects. When the cartilage surface reflection was used for this study to compensate for the effects of the system and transducer, whereas the defocus and diffraction effects were neglected.

From the NDS several parameters were extracted (36):

- The total average power of the NDS (NDS_{avg}, in dB). Only with ExactVu, the signal under 500 μm from the surface was too weak for SAM200Ex
- The slope of attenuation (α_0, in dB/MHz/mm). Only with ExactVu, for the same reason as above.
- The apparent integrated backscatter (AIB) was obtained by averaging the NDS across the transducer's bandwidth, resulting in a depth-dependent profile of the integrated backscattered power. Then The slope (AIB_{slope}, in dB/mm) and intercept (AIB_{I0}, in dB) were extracted from a linear fit.
- The normalized backscattered spectrum (NBS, in dB) was obtained by extrapolating the NDS values within the superficial zone to the surface depth of the sample. Then the slope (NBS_{SS}, in dB/MHz) and intercept (NBS_{I0}, in dB) were extracted from a linear fit. As well as The value of the NBS at the center frequency (NBS_{MF}, in dB).

Additionally, it has been previously described through simulation and experimental data that the location and morphology of peaks within the NDS may correspond to cellular spacing (31). Specifically, it was shown through simulation that peak frequency and cellular spacing had an inverse relationship. Therefore, peaks were detected at each depth within the NDS to be used as features. Peak detection was limited to 100 μm to 250 μm depths beneath the sample surface, corresponding to the superficial zone. Peak detection was also limited to a 25 to 50 MHz bandwidth. This bandwidth was selected because it corresponded to physiologically appropriate cellular spacings according to the relationship defined by Equation 1 in (31). Additionally, because peaks could not always be identified within the bandwidth of ExactVu, peak detection was only carried out in the SAM bandwidth. At each depth between 100 μm to 200 μm, peaks were detected from the spectrum, as shown in Figure 6 (a). The NDS was also

normalized by its maximum amplitude, and all peaks below -15 dB were considered as unreliable and discarded. If multiple peaks were detected at a given depth, the closest peak to the center frequency was selected, 37.5 MHz in this case. The width and prominence of each peak were simultaneously calculated using the peak detection function, as shown in Figure 6 (b). Afterwards, the peak frequencies, widths, and prominences were averaged across depth. The resulting average peak frequency within the 100 to 150 µm depth of the NDS for a sample will be denoted as $NDS_{f_{pk}}^{SAM}$, while the average peak width will be denoted as $NDS_{\Delta f_{pk}}^{SAM}$ and the average peak prominence as $NDS_{prom_{pk}}^{SAM}$. Cell spacing estimated, NDS_{CS}^{SAM}, from frequency peaks was calculated as previously described (31).

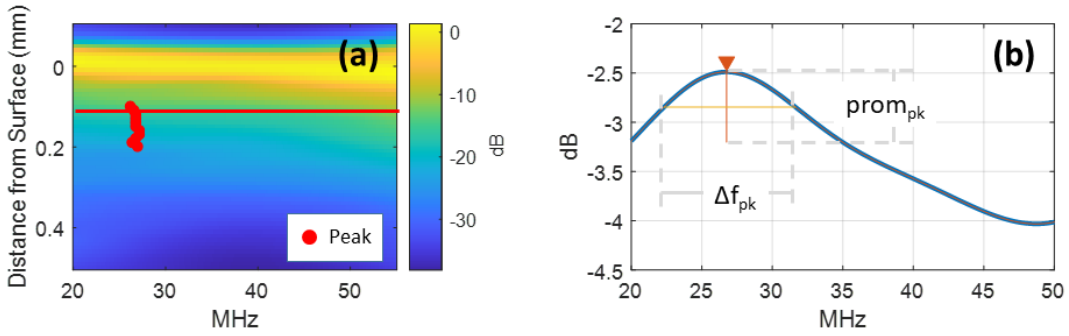

Figure 6: NDS and derived features. (a) NDS with peaks detected within the superficial zone. (b) Spectrum of NDS at given depth indicated by the line in (a). Own Creation.

2.3. Histology

The OCPs plug were then cut into 2 using a scalpel, splitting the OCPs into two half cylinders. One of the half-cylinders was immediately stored in PBS and frozen at -22 °C until use. The other half-cylinders were cut in 2 a second time, splitting the half-cylinders into two-quarters of cylinders. One-quarter of the cylinder was kept for other use, and the second quarter of cylinder was cut into 5 µm sections, stained with Alcian blue and Nuclear fast red-aluminum sulfate, and imaged by light microscopy (LM) (Carl Zeiss Microscopy GmbH, Jena, Germany), to confirm the stage of OA. The severity of degeneration was evaluated according to the Osteoarthritis Research Society International (OARSI) scoring system, specifically using OARSI grade. An OARSI grade of 0 indicates healthy cartilage, while a grade of 6 indicates the most severe OA degeneration (36). The extraction of optical density to assess the Alcian blue staining depletion, and the cell arrangement and density to assess the cell proliferation (clusters), death, and hypertrophy, were performed for each zone (superficial, transitional, and deep zone) using a custom software developed in MATLAB (MATLAB R2018a, MathWorks, Natick, MA). The surface fibrillation and matrix fissures were estimated visually. All

parameters extracted from histology were averaged across three sections per sample. The histology slides were evaluated by a certified clinician for each section. Afterward, the OARSI grade was averaged across three sections. In this study, because samples were collected from patients with early visible signs of OA and donors with no signs of OA, we graded the sample from 0, corresponding to healthy cartilage to 4 corresponding to advanced OA degeneration. Samples were also divided into four groups according to the OARSI grade. Samples with a grade equal to 0 (n=3) composed the group 1 (healthy), samples with a grade between 0.5 and 1,5 (n=17) composed the group 2 (early-stage), samples with a grade between 2 and 3 (n=13) composed the group 3 (mild-stage), and samples with an OARSI grade higher than 3 (n=2) composed the group 4 (advanced stage).

2.4. Magnetic Resonance Imaging acquisition and Data analysis

The half-cylinders stored and frozen at -22 °C were thawed overnight and kept at room temperature for at least one hour in a PBS solution, before scanning with a 3-Tesla small animal MRI benchtop (MRS 3017, MR Solutions, Guildford, UK). Four samples were placed inside a Teflon holder filled with PBS to prevent dehydration, and an additional hole was filled with a fluid to serve as a landmark (Figure 7B). The holder was positioned in the center of a standard mouse coil (Figure 7A), with the surface of the cartilages oriented parallel to the magnetic field B0. The images were acquired along the coronal plane. T1 and T2 morphological and mapping sequences were acquired. The purpose was to compare ultrasound to clinically accessible MRI parameters. T1 relaxation time has been associated with cartilage water content, while T2 has been shown to differentiate between early and advanced stages of OA.

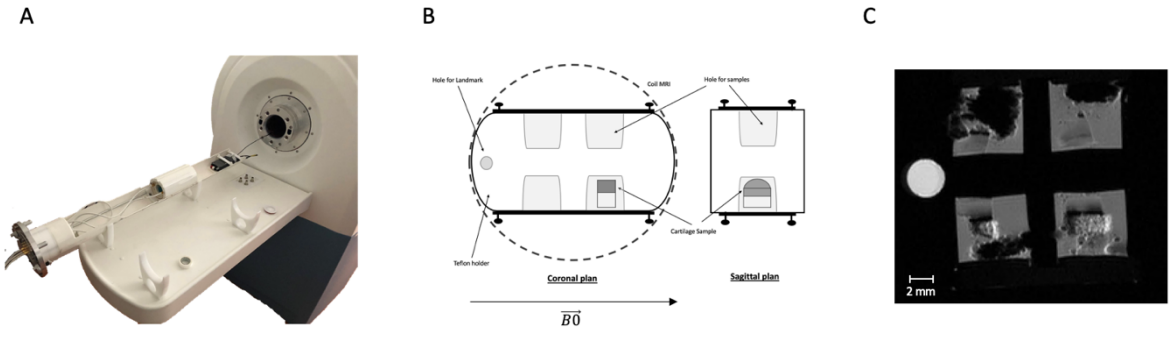

Figure 7: Illustration of the MRI setup (A) 3-Tesla small animal MRI benchtop (MRS 3017, MR Solutions, Guildford, UK). (B) Illustration of the setup for the MRI experiment. (C) Representative T2 mapping of four half-Osteochondral samples (OCPs) at a given slice and echo time. Own Creation.

For MRI analysis, T1 and T2 mapping were calculated from a homogenous region of interest (ROI) of the entire cartilage, using the IR-FSE data and MSME data, respectively. The

T1 parameters were fitted to the mono-exponential relaxation equation (3), using a Levenberg-Marquardt algorithm and all the inversion times:

$$SI = A - SI_0 * e^{-TI/T1} \quad (3)$$

where A represents a constant of magnetization, TI represents the inversion times and SI represents the image signal intensity. The T2 parameters were fitted to the mono-exponential relaxation equation (4), using a Levenberg-Marquardt algorithm and all the echo times:

$$SI = SI_0 * e^{-TE/T2} + C \quad (4)$$

where C represents a constant of magnetization, TE represents the echo times and SI represents the image signal intensity. Due to the shape of the samples, half of the cylinder, the ROIs were individually defined on the slice corresponding to the central area of the cartilage and compared with the histology section to avoid inclusion of subchondral bone or artifacts. All parameters were computed using a custom software built on MATLAB (MATLAB R2018a, MathWorks, Natick, MA).

2.5. Statistics

First, descriptive statistics were used to compare similar parameters extracted from different modalities. Afterward, we classified the parameters into two types of data, categorical or numerical. Then, for each numerical parameter, an Anderson-Darling test was conducted to assess the sample distribution and check if a parametric or non-parametric test should be used. As well as a Q-Q plot to visualize the results. In addition, one-way ANOVA parametric analyses of variance were completed to determine the inequity of the OARSI groups for the MRI parameters. Then, a post-hoc multi-comparison test, using Tukey-Kramer's method, was used to determine which groups are different from the others, when the ANOVA was significant. The relation between all the quantitative parameters from different imaging techniques (MRI, SAM, and ExactVu) and the OARSI grade or Histological parameters were assessed by using spearman's correlation analysis or the pearson correlation coefficient, depending on whether the quantitative parameter follows a normal distribution. Finally, the influence of these quantitative parameters was evaluated by performing a multivariate stepwise linear regression, to select the variables for each imaging technique with significant associations with the OARSI grade. When more than two significant parameters were retrieved, these variables were orthogonalized by means of principal component analysis and partial least squares (PLS) regression analysis using two components and 3-fold cross-validation to avoid overfitting.

Statistical tests were performed using the Statistics Toolbox of Matlab R2019 (MathWorks, Natick, MA) and considered significant for p-value < 0.05.

3 Results

3.1. Descriptive statistics of parameters from histology and ultrasound

Table 2: Averages and standard deviations of LM-based parameters, and QUS-based spacing estimation from SAM200Ex for each OARSI grade. SZ: superficial zone. Own Creation.

OARSI grade	**LM Optical density***	**LM Cell density***	LM spacing (µm) (SZ)	NDS_{CS}^{SAM} (µm) (SZ)
0	162 ± 8	685 ± 134	20.17 ± 1.1	28.2 ± 1.7
0.5	156 ± 8	1146 ± 540	20.04 ± 0.9	20.7 ± 7.0
1	158 ± 14	899 ± 245	19.19 ± 1.1	21.6 ± 7.2
1.5	157 ± 13	712 ± 312	20.36 ± 0.1	20.7 ± 4.0
2	166 ± 11	572 ± 154	20.46 ± 1.3	23.0 ± 8.6
2.5	170 ± 10	723 ± 145	20.58 ± 1.3	29.9 ± 14.1
3	173 ± 14	587 ± 269	23.26 ± 4.4	NaN
4	187 ± 8	243 ± 112	23.12 ± 0.3	NaN

* Indicates significant differences between the OARSI grade groups.

The average LM-based optical density, cell density, and cell spacing for each OARSI grade are reported in Table 2. Along with the average cell density extracted from the SAM200Ex. We could observe a diminution of the optical density in the early grade of OA in comparison with the samples without sign of destruction (OARSI = 0), followed by an augmentation in the most advanced cases (OARSI ≥ 2). In addition, the cell density was larger in the first grades of OA, before decreasing as the degeneration was advanced (Figure 8). For the LM-based spacing, we observed an augmentation for the cartilage samples with an OARSI grade superior to 2.5 as opposed to the other OA grades. The augmentation of the cell spacing is observable earlier, OARSI grade superior to 1.5, for the parameters extracted from SAM200Ex. However, only the LM-based optical density and cell density were significantly correlated to the OA grades.

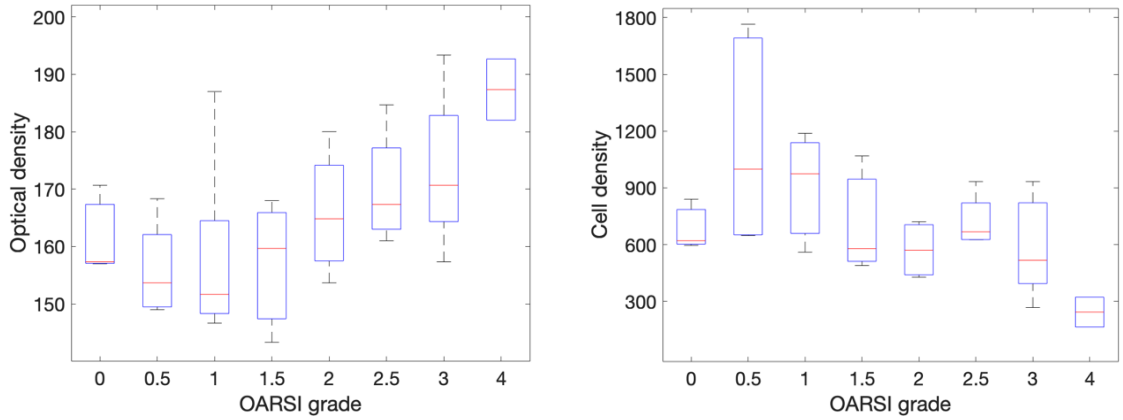

Figure 8: Box plots of (a) the LM-based optical density values and (b) the LM-based cell density values with respects to the OARSI grade of the samples. The optical density first decreases before to increase as the OA grade is advanced. The cell density first increases before to decrease as the OA grade is advanced. Own Creation.

3.2. Samples Distribution

According to the Q-Q plots and Anderson-Darling tests, the parameters following or not following a normal distribution could be assumed. The histological parameter cell density rejected the null hypothesis of the test, assuming that this parameter doesn't follow a normal distribution, while optical density and spacing did not reject the null hypothesis of the test and follow a normal distribution. The MRI parameters (T1 and T2) followed a normal distribution. Some ultrasound parameters, such as AIB_{slope} extracted from ExactVu and Integrated reflection coefficient (IRC), AIB_{slope}, AIB_{I0} extract from SAM200Ex follow a normal distribution, while others, such as IRC and AIB_{I0} extracted from ExactVu do not follow a normal distribution. Figure 9 is a representation of two Q-Q plots examples of the parameters tested, one following a normal distribution and the other no.

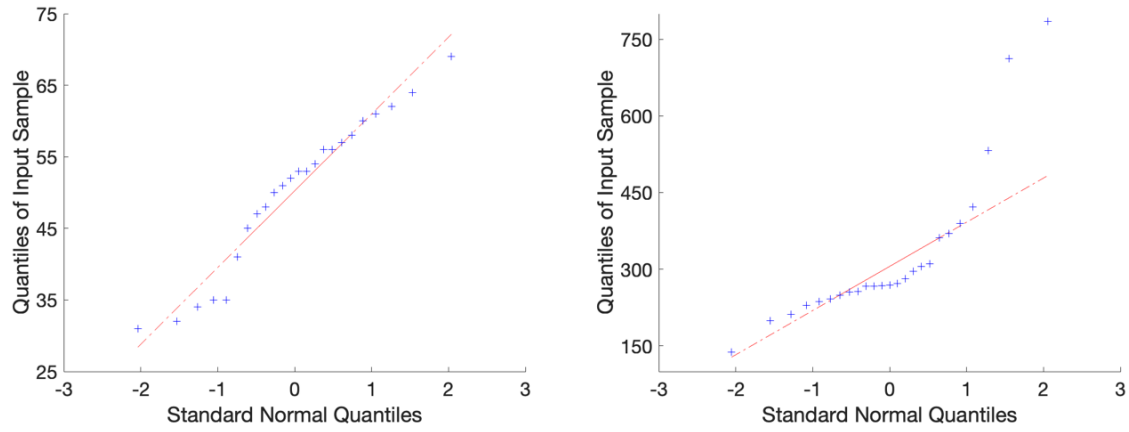

Figure 9: Q-Q plots of (a) T2 MRI data versus Standard normal and of (b) Histological cell density from the deep zone versus Standard normal. The blue scatterplot represents the dataset of the parameter. The solid red line represents the quantile-quantile plot, connecting the first and third quartiles of the data. The dashed red line extends the solid red line to the ends of the data. Own Creation.

3.3. Ultrasound

The parameters that were derived from ExactVu and significantly correlated with OARSI grade were AIB_{slope} with a ρ of 0.73 and NDS_{avg} with a ρ of 0.47 (36). For SAM200Ex parameters, only IRC was significantly correlated with OARSI grade, with a ρ of -0.56 (36). The results of the correlation analysis for the AIB_{slope} and AIB_{I0} derived from ExactVu and SAM200Ex, with the optical and cell densities in the superficial, transitional zone and the full samples are given in Table 3. The AIB_{slope} extracted from ExactVu was moderately correlated to the cell densities of the full sample, the superficial and transitional layer. The AIB_{I0} extracted from both systems was moderately correlated to the cell density of the full sample and the transitional layer. The AIB_{slope} extracted from the SAM200Ex was significantly correlated to the cell densities of the full sample, the superficial and transitional layer, with the highest ρ, -0.68, -0.69, and -0.57, respectively.

Table 3: Correlation of AIB_{slope} and AIB_{I0} derived from ExactVu and SAM200Ex with Optical and Cell densities. SZ: superficial zone, TZ: transitional zone, FS: full sample. Own Creation.

Parameters		ExactVu		SAM200Ex	
		AIB_{slope}	AIB_{I0}	AIB_{slope}	AIB_{I0}
Cell Density SZ	p-value	**0.046***	0.08	**0.002***	0.1
	ρ	-0.39	0.35	-0.57	0.33
Cell Density TZ	p-value	**0.028***	**0.02***	**0.001***	**0.04***
	ρ	-0.43	0.47	-0.69	0.40
Cell Density FS	p-value	**0.025***	**0.025***	**0.001***	**0.05***
	ρ	-0.44	0.44	-0.68	0.40
Optical Density SZ	p-value	0.19	0.09	0.11	0.24
	ρ	0.26	-0.34	0.32	-0.24
Optical Density TZ	p-value	0.35	**0.01***	**0.007***	**0.03***
	ρ	0.19	-0.50	0.51	-0.44
Optical Density FS	p-value	0.28	**0.04***	**0.04***	0.11
	ρ	0.15	-0.41	0.41	-0.32

3.4. Magnetic Resonance Imaging

The groups averaging of the T2 relaxation times are significantly different (p-value: $6x10^{-6}$). We can observe an increase of the T2 values with the stage of the degradation (Figure 10). Then the post hoc multi-comparison test showed that the groups 1 (healthy) and 2 (early stage) are

significantly different to group 3 and 4. The groups 3 (mild stage) and 4 (advanced stage) are significantly different to all groups.

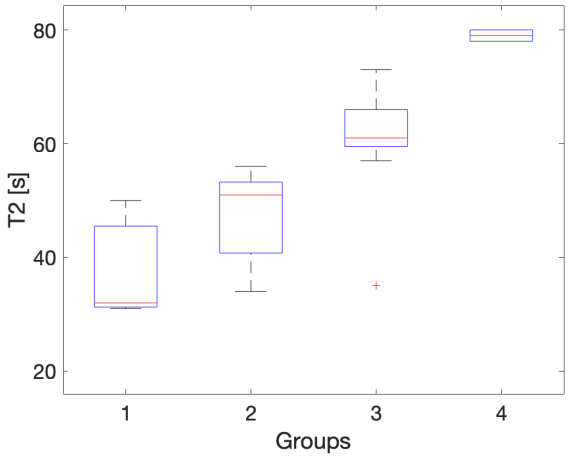

Figure 10: Box plot of the T2 relaxation time values with respect to the OARSI groups. Group 1: healthy, Group 2: early stage, Group 3: mild stage, Group 4: advanced stage. The T2 values increase as the degeneration is advanced. Own Creation.

3.5. Multi-Parameter and Multi-modal Correlation

The results of PLS regression with OARSI grade, using two components, are given in Table 4 (36). The combination of all modalities (ExactVu, SAM200Ex, and MRI) and ExactVu / MRI had the highest correlation, with a ρ of 0.82. Followed by the ExactVu and MRI, with both a ρ of 0.75. The plots of the predicted OARSI grades, using PLS regression with the different modalities' parameters combination, against the true OARSI grades are given in Figure 11.

Table 4: Results from PLS regression using two components of different modalities and combination. Own Creation.

Modalities	p-value	R^2	ρ
ExactVu	**<0.001***	0.53	0.75
SAM200Ex	**<0.001***	0.36	0.62
MRI	**<0.001****	0.53	0.75
ExactVu / SAM200Ex	**<0.001***	0.53	0.73
ExactVu / MRI	**<0.001***	0.68	0.82
All modalities	**<0.001***	0.67	0.82

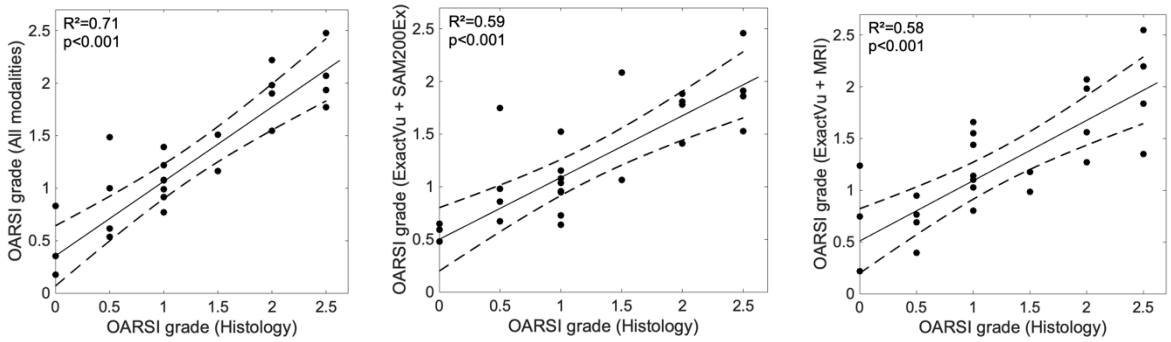

Figure 11: Regression plots of OARSI grade against (a) all modalities, (b) Ultrasound modalities, (c) MRI and ExactVu systems. Dotted line indicates the 95% confidence intervals. Own Creation.

4 Discussion

This study confirmed that quantitative ultrasound parameters extracted from high-frequency systems are sensitive to early signs of osteoarthritis. The results revealed significant correlations between the IRC derived from a scanning acoustic microscope with a single-element spherically-focused transducer and OARSI grade, with a maximum ρ of 0.56 achieved (36). Moreover, the AIB_{slope} derived from a clinical ultrasound system, with a linear array transducer, was correlated to OARSI grade, with a ρ of 0.73 (36). This result is higher than the correlation obtained with the T2 relation time from the MRI, with a maximum ρ of 0.62 (36). In addition, the T2s were also significantly different between the OA groups. The early, mild, and advanced groups were significantly different from each other (p-value < 0.001). While the healthy group was significantly different from the mild and advanced group (p-value < 0.001). Finally, the combinations of the quantitative parameters extracted from these different modalities were also significantly correlated to OARSI grade, with a maximum ρ of 0.82 for the combination of all the modalities, a maximum ρ of 0.73 for the combination ExactVu/SAME200Ex, and a maximum ρ of 0.82 for the combination ExactVu/MRI.

Ultrasound backscattering parameters on healthy and artificially degraded articular cartilage were broadly analyzed. In this study, the slope of the apparent integrated backscatter (AIB_{slope}), extracted from the clinical approved ExactVu system was correlated to the early and mild grade (OARSI grade <3), and to the cell density of the full sample and the different layers separately. Previous studies using a single-element spherically-focused transducer (29, 31, 37), demonstrated that AIB was related to the collagen orientation, the cell density, and the different grades of OA. In addition, the SAM200Ex system showed a significant correlation between the surface parameter IRC and the early stages of OA (OARSI grade < 3) (36). This is in line with

prior work, applying the same method (27), and attributing the increase of IRC to the incoherent waves scattered by the fibrillated surface (30).

Nevertheless, the AIB_{slope} extracted from the SAM200Ex system did not correlate the early stage of degeneration, but significantly correlated to the cell density, in agreement with a previous study that has shown no statistical differences in AIB with early OA grades, but a moderate correlation to the cell density (28). The cell spacing estimation based on the resonance peak frequency (31), was also investigated in this present study. As described by Rohrbach et al., the quantitative ultrasound spacing estimation, using high frequency and in-silico cartilage models, was a promising indicator for early degeneration changes. However, we were not able to confirm these findings in a larger amount of ex-vivo samples.

The correlation between QUS parameters from a clinical ultrasound system was comparable to MRI parameters ($\rho = 0.75$). The current study revealed that T2 is a good MRI feature to predict the different stages of OA (36). This is consistent with several previous studies that have shown that T2 relaxation time is related to different contents involved in the organization of the cartilage. It is well known that the early stages of OA present a disruption of the collagen network, which provokes a modification of the cartilage water. And these studies suggest that T2 quantifies collagen network integrity and water contents (20, 21). But also, as described by Rautiainen et al., T2 values were able to differentiate early and advanced stages of osteoarthritis and were correlated to histological results.

The statistical differences provided by the combination of parameters and modalities suggest also that with just two parameters as predictors, we can classify the early stages of OA. This is in line with the results suggested by Männicke et al., and demonstrates the potential of using combinations of QUS parameters to classify the degradation of OA (32). Moreover, the results showed that quantitative MRI and quantitative ultrasound can be used complementarily in the detection of osteoarthrosis in its early stage. The ultrasound system can provide a good, non-invasive, fast, and low-cost support to MRI in the diagnosis and treatment planning of degenerative cartilage diseases.

The few limitations of the current study must be mentioned. The region of interest where the QUS parameters were extracted is not exactly the same between the ExactVu systems, the SAM200Ex, the MRI system, and the histology, introducing possible variation in the results. Another limitation is the normalization method of the backscattered spectra. In the current study, the surface of each sample was used to normalize, while in the previous studies they used a reference phantom or a planar reflector, which introduced a bias (36). Explaining why some

QUS parameters did not correlate with early stages of OA, while prior studies have demonstrated the opposite (31). However, the extraction of significant QUS parameters without reference calibration can be a benefit for clinical settings. We used a sound speed of 1590 m/s for all samples when it is well known that the speed of sound is slightly different between healthy and degenerated cartilage. Even though if recalculating the parameters with different sound speeds did not affect the results. Finally, the conditions of the *ex-vivo* measurement differ from their normal physiological environment. The presence of skin and subcutaneous tissues may affect the results for future in-vivo studies.

Correlating the same QUS parameters to the different stages of OA might be more challenging. Due to the presence of skin and subcutaneous tissues that would significantly increase the attenuation of sound waves. However, a previous study demonstrated the possibility of imaging knee cartilage with ultrasound systems (38). With a better penetration depth, the sensitivity of the QUS parameters extracted from ExactVu to OA should be investigated *in-vivo*. Different parameters were significantly correlated to the progression of OA. The IRC for ExactVu and AIB_{slope} for SAM200Ex, suggesting a link between the sensitivity of the parameters to OA and the transducer used. For AIB_{slope}, the following hypothesis can be raised: AIB_{slope} contained more information derived from ExactVu, due to its larger depth of field and lower frequency, offering less attenuation over depth. Explaining the no statistically significant differences shown in prior studies (28). For IRC, it can be explained by the lower frequencies of the ExactVu, incapable of capturing the superficial fibrillation present in early OA.

In conclusion, this *ex-vivo* study demonstrated that a high-frequency clinical ultrasound system with a linear array transducer is a promising device to predict early osteoarthritis stages, with results comparable to MRI. However, ultrasound has advantages over MRI, being low-cost and easily accessible. Furthermore, the combination of these two systems showed a strong significant correlation with the early OA grade. Future studies should focus on the investigation of the assessment of early *in-vivo* OA, using quantitative ultrasound.

5 References

1. Sophia Fox AJ, Bedi A, Rodeo SA. The basic science of articular cartilage: structure, composition, and function. Sports Health. 2009;1(6):461-8.

2. Buckwalter JA, Mankin HJ, Grodzinsky AJ. Articular cartilage and osteoarthritis. Instr Course Lect. 2005;54:465-80.

3. Kloppenburg M, Berenbaum F. Osteoarthritis year in review 2019: epidemiology and therapy. Osteoarthritis Cartilage. 2020;28(3):242-8.

4. Safiri S, Kolahi AA, Smith E, Hill C, Bettampadi D, Mansournia MA, Hoy D, Ashrafi-Asgarabad A, Sepidarkish M, Almasi-Hashiani A, Collins G, Kaufman J, Qorbani M, Moradi-Lakeh M, Woolf AD, Guillemin F, March L, Cross M. Global, regional and national burden of osteoarthritis 1990-2017: a systematic analysis of the Global Burden of Disease Study 2017. Ann Rheum Dis. 2020;79(6):819-28.

5. Fuchs J, Kuhnert R, Scheidt-Nave C. 12-month prevalence of osteoarthritis in Germany. Robert Koch-Institut, Epidemiologie und Gesundheitsberichterstattung; 2017.

6. Nations TU. World Population in 2300. Population and Development Review. 2004;30(1):181-7.

7. GBD 2017 Disease and Injury Incidence and Prevalence Collaborators. Global, regional, and national incidence, prevalence, and years lived with disability for 354 diseases and injuries for 195 countries and territories, 1990-2017: a systematic analysis for the Global Burden of Disease Study 2017. The Lancet. 2018;392(10159):1789-858.

8. Salmon JH, Rat AC, Sellam J, Michel M, Eschard JP, Guillemin F, Jolly D, Fautrel B. Economic impact of lower-limb osteoarthritis worldwide: a systematic review of cost-of-illness studies. Osteoarthritis Cartilage. 2016;24(9):1500-8.

9. Rabenberg M. Themenheft 54 "Arthrose". Robert Koch-Institut; 2013.

10. Cameron KL, Hsiao MS, Owens BD, Burks R, Svoboda SJ. Incidence of physician-diagnosed osteoarthritis among active duty United States military service members. Arthritis Rheum. 2011;63(10):2974-82.

11. Courties A, Sellam J, Berenbaum F. Metabolic syndrome-associated osteoarthritis. Curr Opin Rheumatol. 2017;29(2):214-22.

12. Mansfield JC, Mandalia V, Toms A, Winlove CP, Brasselet S. Collagen reorganization in cartilage under strain probed by polarization sensitive second harmonic generation microscopy. J R Soc Interface. 2019;16(150):20180611.

13. Kraus VB, Blanco FJ, Englund M, Karsdal MA, Lohmander LS. Call for standardized definitions of osteoarthritis and risk stratification for clinical trials and clinical use. Osteoarthritis Cartilage. 2015;23(8):1233-41.

14. Pritzker KP, Gay S, Jimenez SA, Ostergaard K, Pelletier JP, Revell PA, Salter D, van den Berg WB. Osteoarthritis cartilage histopathology: grading and staging. Osteoarthritis Cartilage. 2006;14(1):13-29.

15. Guermazi A, Hayashi D, Eckstein F, Hunter DJ, Duryea J, Roemer FW. Imaging of osteoarthritis. Rheum Dis Clin North Am. 2013;39(1):67-105.

16. Mathiessen A, Cimmino MA, Hammer HB, Haugen IK, Iagnocco A, Conaghan PG. Imaging of osteoarthritis (OA): What is new? Best Pract Res Clin Rheumatol. 2016;30(4):653-69.

17. Liukkonen J, Lehenkari P, Hirvasniemi J, Joukainen A, Viren T, Saarakkala S, Nieminen MT, Jurvelin JS, Toyras J. Ultrasound arthroscopy of human knee cartilage and subchondral bone in vivo. Ultrasound Med Biol. 2014;40(9):2039-47.

18. Siemieniuk RAC, Harris IA, Agoritsas T, Poolman RW, Brignardello-Petersen R, Van de Velde S, Buchbinder R, Englund M, Lytvyn L, Quinlan C, Helsingen L, Knutsen G, Olsen NR, Macdonald H, Hailey L, Wilson HM, Lydiatt A, Kristiansen A. Arthroscopic surgery for degenerative knee arthritis and meniscal tears: a clinical practice guideline. BMJ. 2017;357:j1982.

19. Hafezi-Nejad N, Demehri S, Guermazi A, Carrino JA. Osteoarthritis year in review 2017: updates on imaging advancements. Osteoarthritis Cartilage. 2018;26(3):341-9.

20. Herzen J, Karampinos DC, Foehr P, Birnbacher L, Viermetz M, Burgkart R, Baum T, Lohoefer F, Wildgruber M, Schilling F, Willner M, Marschner M, Noel PB, Rummeny EJ, Pfeiffer F, Jungmann PM. 3D grating-based X-ray phase-contrast computed tomography for high-resolution quantitative assessment of cartilage: An experimental feasibility study with 3T MRI, 7T MRI and biomechanical correlation. PLoS One. 2019;14(2):e0212106.

21. Hanninen NE, Nykanen O, Prakash M, Hanni M, Nieminen MT, Nissi MJ. Orientation anisotropy of quantitative MRI parameters in degenerated human articular cartilage. J Orthop Res. 2020.

22. Rautiainen J, Nieminen MT, Salo EN, Kokkonen HT, Mangia S, Michaeli S, Grohn O, Jurvelin JS, Toyras J, Nissi MJ. Effect of collagen cross-linking on quantitative MRI parameters of articular cartilage. Osteoarthritis Cartilage. 2016;24(9):1656-64.

23. Watanabe A, Wada Y, Obata T, Ueda T, Tamura M, Ikehira H, Moriya H. Delayed gadolinium-enhanced MR to determine glycosaminoglycan concentration in reparative cartilage after autologous chondrocyte implantation: preliminary results. Radiology. 2006;239(1):201-8.

24. Laugier P. Bone quantitative ultrasound: Springer; 2014.

25. Csiba Ls, Baracchini C. Manual of neurosonology2016.

26. Oo WM, Linklater JM, Daniel M, Saarakkala S, Samuels J, Conaghan PG, Keen HI, Deveza LA, Hunter DJ. Clinimetrics of ultrasound pathologies in osteoarthritis: systematic literature review and meta-analysis. Osteoarthritis Cartilage. 2018;26(5):601-11.

27. Schone M, Mannicke N, Gottwald M, Gobel F, Raum K. 3-d high-frequency ultrasound improves the estimation of surface properties in degenerated cartilage. Ultrasound Med Biol. 2013;39(5):834-44.

28. Mannicke N, Schone M, Gottwald M, Gobel F, Oelze ML, Raum K. 3-D high-frequency ultrasound backscatter analysis of human articular cartilage. Ultrasound Med Biol. 2014;40(1):244-57.

29. Mannicke N, Schone M, Liukkonen J, Fachet D, Inkinen S, Malo MK, Oelze ML, Toyras J, Jurvelin JS, Raum K. Species-Independent Modeling of High-Frequency Ultrasound Backscatter in Hyaline Cartilage. Ultrasound Med Biol. 2016;42(6):1375-84.

30. Cherin E, Saied A, Laugier P, Netter P, Berger G. Evaluation of acoustical parameter sensitivity to age-related and osteoarthritic changes in articular cartilage using 50-MHz ultrasound. Ultrasound Med Biol. 1998;24(3):341-54.

31. Rohrbach D, Inkinen SI, Zatloukalova J, Kadow-Romacker A, Joukainen A, Malo MK, Mamou J, Toyras J, Raum K. Regular chondrocyte spacing is a potential cause for coherent ultrasound backscatter in human articular cartilage. J Acoust Soc Am. 2017;141(5):3105.

32. Mannicke N, Schone M, Oelze M, Raum K. Articular cartilage degeneration classification by means of high-frequency ultrasound. Osteoarthritis Cartilage. 2014;22(10):1577-82.

33. Leicht S, Raum K. Acoustic impedance changes in cartilage and subchondral bone due to primary arthrosis. Ultrasonics. 2008;48(6-7):613-20.

34. Rohrbach D. Quantitative ultrasound in transverse transmission for bone quality assessment and monitoring fracture healing: Humboldt-Universität zu Berlin, Mathematisch-Naturwissenschaftliche Fakultät I; 2013.

35. Iori G, Du J, Hackenbeck J, Kilappa V, Raum K. Estimation of Cortical Bone Microstructure from Ultrasound Backscatter. IEEE Trans Ultrason Ferroelectr Freq Control. 2020;PP.

36. Lye TH, Gachouch O, Renner L, Elezkurtaj S, Cash H, Messroghli D, Raum K, Mamou J. Quantitative Ultrasound Assessment of Early Osteoarthritis in Human Articular Cartilage Using a High-Frequency Linear Array Transducer. Ultrasound Med Biol. 2022.

37. Inkinen SI, Liukkonen J, Malo MK, Viren T, Jurvelin JS, Toyras J. Finite difference time domain model of ultrasound propagation in agarose scaffold containing collagen or chondrocytes. J Acoust Soc Am. 2016;140(1):1.

38. Podlipska J, Koski JM, Kaukinen P, Haapea M, Tervonen O, Arokoski JP, Saarakkala S. Structure-symptom relationship with wide-area ultrasound scanning of knee osteoarthritis. Sci Rep. 2017;7:44470.

Statutory Declaration

"I, Omar Gachouch, by personally signing this document in lieu of an oath, hereby affirm that I prepared the submitted dissertation on the topic "Ultrasound based histomorphology for non-invasive grading of early cartilage degeneration / Ultraschallbasierte Histomorphologie zur nicht-invasiven Klassifizierung der frühen Knorpeldegeneration", independently and without the support of third parties, and that I used no other sources and aids than those stated.
All parts which are based on the publications or presentations of other authors, either in letter or in spirit, are specified as such in accordance with the citing guidelines. The sections on methodology (in particular regarding practical work, laboratory regulations, statistical processing) and results (in particular regarding figures, charts and tables) are exclusively my responsibility.

Furthermore, I declare that I have correctly marked all of the data, the analyses, and the conclusions generated from data obtained in collaboration with other persons, and that I have correctly marked my own contribution and the contributions of other persons (cf. declaration of contribution). I have correctly marked all texts or parts of texts that were generated in collaboration with other persons.

My contributions to any publications to this dissertation correspond to those stated in the below joint declaration made together with the supervisor. All publications created within the scope of the dissertation comply with the guidelines of the ICMJE (International Committee of Medical Journal Editors; www.icmje.org) on authorship. In addition, I declare that I shall comply with the regulations of Charité – Universitätsmedizin Berlin on ensuring good scientific practice.

I declare that I have not yet submitted this dissertation in identical or similar form to another Faculty.

The significance of this statutory declaration and the consequences of a false statutory declaration under criminal law (Sections 156, 161 of the German Criminal Code) are known to me."

Date: 22.05.2022 Signature

Declaration of contribution to the publication

Omar Gachouch contributed the following to the below publication:

Publication: T. H. Lye*, O. Gachouch*, L. Renner, S. Elezkurtaj, H. Cash, D. Messroghli, K. Raum, and J. Mamou, Quantitative Ultrasound Assessment of Early Osteoarthritis in Human Articular using a High-Frequency Linear Array Transducer, Ultrasound in Medicine & Biology, 2022

* These authors contributed equally.

Contribution in detail:

Experiments:
- Design of the ultrasound protocols under the supervision of Prof. Dr. Kay Raum.
- Design of the histology protocol.
- Design of the magnetic resonance imaging protocol under the supervision of Dr. Daniel Messroghli.
- Sample collection and preparation.
- Acquisition of ultrasound, magnetic resonance imaging and histology data.

Data analysis:
- Development and implementation of the image processing, analysis, and interpretation of the histology data under the supervision of Prof. Dr Kay Raum.
- Development and implementation of the image processing tools, analysis, and interpretation of the magnetic resonance imaging data under the supervision of Prof. Dr. Kay Raum.
- Development and implementation of the signal processing tools, analysis, and interpretation of the ultrasound data with Dr. Theresa H. Lye and under the supervision of Prof. Dr. Kay Raum and Dr. Jonathan Mamou.
- Statistical expertise with Dr. Theresa H. Lye and under the supervision of Prof. Dr. Kay Raum and Dr. Jonathan Mamou.

Manuscript:
- Drafting of all the sections of the article (introduction, methods, results, discussion, conclusions) with Dr. Theresa H. Lye.
- I created the figures 1, 2, 3, and 6. I created the tables 1, 3, and 4.
- Review and editing of the article by all authors.

_____

Signature, date and stamp of first supervising university professor / lecturer

_____

Signature of doctoral candidate

Declaration of contribution to the publication

Theresa H. Lye contributed the following to the below publication:

Publication: T. H. Lye*, O. Gachouch*, L. Renner, S. Elezkurtaj, H. Cash, D. Messroghli, K. Raum, and J. Mamou, Quantitative Ultrasound Assessment of Early Osteoarthritis in Human Articular using a High-Frequency Linear Array Transducer, Ultrasound in Medicine & Biology, 2022

* These authors contributed equally.

Contribution in detail:

Data analysis:

- Development and implementation of the signal processing tools, analysis, and interpretation of the ultrasound data with Omar Gachouch and under the supervision of Prof. Dr. Kay Raum and Dr. Jonathan Mamou.
- Statistical expertise with Omar Gachouch and under the supervision of Prof. Dr. Kay Raum and Dr. Jonathan Mamou.

Manuscript:

- Drafting of the article with Omar Gachouch.
- Review and editing of the article by all authors.

_____

Signature, date and stamp of first supervising university professor / lecturer

_____

Signature of doctoral candidate

Extract from the Journal summary list

Journal Data Filtered By: **Selected JCR Year: 2020** Selected Editions: SCIE,SSCI
Selected Categories: **'ACOUSTICS'** Selected Category Scheme: WoS
Gesamtanzahl: 32 Journale

Rank	Full Journal Title	Total Cites	Journal Impact Factor	Eigenfactor Score
1	ULTRASONICS SONOCHEMISTRY	26,178	7.491	0.021770
2	ULTRASOUND IN OBSTETRICS & GYNECOLOGY	18,164	7.299	0.018820
3	ULTRASCHALL IN DER MEDIZIN	2,911	6.548	0.003340
4	IEEE-ACM Transactions on Audio Speech and Language Processing	4,568	3.919	0.008150
5	JOURNAL OF SOUND AND VIBRATION	41,178	3.655	0.025350
6	JOURNAL OF VIBRATION AND CONTROL	6,405	3.095	0.006790
* 7	ULTRASOUND IN MEDICINE AND BIOLOGY	12,787	2.998	0.011140
8	ULTRASONICS	8,026	2.890	0.006980
9	JOURNAL OF LOW FREQUENCY NOISE VIBRATION AND ACTIVE CONTROL	1,084	2.837	0.001490
10	IEEE TRANSACTIONS ON ULTRASONICS FERROELECTRICS AND FREQUENCY CONTROL	11,100	2.725	0.006820
11	APPLIED ACOUSTICS	9,042	2.639	0.008530
12	JOURNAL OF ULTRASOUND IN MEDICINE	9,425	2.153	0.008530
13	WAVE MOTION	2,667	2.020	0.002580
14	SPEECH COMMUNICATION	3,575	2.017	0.003190
15	JOURNAL OF THE ACOUSTICAL SOCIETY OF AMERICA	49,404	1.840	0.021990
16	PHONETICA	806	1.759	0.000600

Rank	Full Journal Title	Total Cites	Journal Impact Factor	Eigenfactor Score
17	Medical Ultrasonography	1,089	1.611	0.001600
18	JOURNAL OF VIBRATION AND ACOUSTICS-TRANSACTIONS OF THE ASME	3,974	1.583	0.002960
19	ULTRASONIC IMAGING	1,055	1.578	0.000510
20	EURASIP Journal on Audio Speech and Music Processing	439	1.558	0.000660
21	SHOCK AND VIBRATION	4,881	1.543	0.007040
22	Acoustics Australia	360	1.500	0.000380
23	Journal of Theoretical and Computational Acoustics	90	1.171	0.000220
24	International Journal of Aeroacoustics	497	1.115	0.000790
25	Archives of Acoustics	617	0.913	0.000570
26	JOURNAL OF CLINICAL ULTRASOUND	2,488	0.910	0.001490
27	ACOUSTICAL PHYSICS	956	0.856	0.000690
28	JOURNAL OF THE AUDIO ENGINEERING SOCIETY	1,395	0.833	0.000670
29	ACTA ACUSTICA UNITED WITH ACUSTICA	2,536	0.762	0.001870
30	International Journal of Acoustics and Vibration	338	0.581	0.000340
31	NOISE CONTROL ENGINEERING JOURNAL	582	0.466	0.000410
32	ACTA ACUSTICA	141	Not Available	0.000020

Copyright © 2021 Clarivate Analytics

https://doi.org/10.1016/j.ultrasmedbio.2022.03.006

https://doi.org/10.1016/j.ultrasmedbio.2022.03.006

https://doi.org/10.1016/j.ultrasmedbio.2022.03.006

https://doi.org/10.1016/j.ultrasmedbio.2022.03.006

https://doi.org/10.1016/j.ultrasmedbio.2022.03.006

https://doi.org/10.1016/j.ultrasmedbio.2022.03.006

https://doi.org/10.1016/j.ultrasmedbio.2022.03.006

https://doi.org/10.1016/j.ultrasmedbio.2022.03.006

https://doi.org/10.1016/j.ultrasmedbio.2022.03.006

https://doi.org/10.1016/j.ultrasmedbio.2022.03.006

https://doi.org/10.1016/j.ultrasmedbio.2022.03.006

https://doi.org/10.1016/j.ultrasmedbio.2022.03.006

My curriculum vitae does not appear in the electronic version of my paper for reasons of data protection.

List of publication

Conferences

Theresa Lye, Omar Gachouch, Lisa Renner, Kay Raum, Jonathan Mamou, “Quantitative Ultrasound Characterization of Human Articular Cartilage” in 2020 IEEE International Ultrasonics Symposium (IUS)

Article

T. H. Lye[1], O. Gachouch[1] L. Renner, S. Elezkurtaj, H. Cash5 D. Messroghli, K. Raum, and J. Mamou, “Quantitative Ultrasound Assessment of Early Osteoarthritis in Human Articular using a High-Frequency Linear Array Transducer” in Ultrasound in Medicine and Biology, 2022.

Impact Factor: 2.998

1 These authors contributed equally.

Acknowledgements

I would start to thank my doctoral supervisor Prof. Dr. Kay Raum for his support, guidance, and to give me the opportunity to perform this research in his group. I would also like to thank my second supervisor Dr. Jonathan Mamou and my mentor Dr. Lisa Renner for their advice and guidance during my 3 years of studies. Their experience in science and encouragements were essential all along my development as a researcher. I would like to expressing my gratitude to the Berlin-Brandenburg School for Regenerative Therapies of the Charité Universitätsmedizin Berlin, where I conducted my PhD research and all people I met there.

I would like to specially thank my colleagues Huong, Mathis, Tim, Nirina, Maria, Regina, and Urszula for all the memorable time we spent together, their encouragement and constructive discussion. I also extend my particularly thank to Theresa with whom I conducted the analyses and interpretation of the data of this study, and to my collaborators Dr. Daniel Messroghli and Dr. Hannes Cash. Their helpful comments and productive discussions contributed to the success of this study. Many thanks to Urszula, Sabine, Gabriela, Nicola and Daniel for their technical support during my work. Thank you Katharina, Jean, Kay, Miguel, and Daniela for proof reading this thesis.

Finally, I want to thank my whole family for their unlimited support in all aspect of my life.